Diet-Induced Obesity Increases Tumor Growth and Promotes Anaplastic Change in Thyroid Cancer in a Mouse Model

Won Gu Kim, Jeong Won Park, Mark C. Willingham, and Sheue-yann Cheng

Laboratory of Molecular Biology, Center for Cancer Research, National Cancer Institute, Bethesda, Maryland 20892-4264

Recent epidemiological studies provide strong evidence suggesting obesity is a risk factor in several cancers, including thyroid cancer. However, the molecular mechanisms by which obesity increases the risk of thyroid cancer are poorly understood. In this study, we evaluated the effect of diet-induced obesity on thyroid carcinogenesis in a mouse model that spontaneously develops thyroid cancer ($Thrb^{PV/PV}Pten^{+/-}$ mice). These mice harbor a mutated thyroid hormone receptor-β (denoted as PV) and haplodeficiency of the *Pten* gene. A high-fat diet (HFD) efficiently induced the obese phenotype in $Thrb^{PV/PV}Pten^{+/-}$ mice after 15 weeks. Thyroid tumor growth was markedly greater and survival was significantly lower in $Thrb^{PV/PV}Pten^{+/-}$ mice fed an HFD than in controls fed a low-fat diet (LFD). The HFD increased thyroid tumor cell proliferation by increasing the protein levels of cyclin D1 and phosphorylated retinoblastoma protein to propel cell cycle progression. Histopathological analysis showed that the frequency of anaplasia of thyroid cancer was significantly greater (2.6-fold) in the HFD group than the LFD group. The HFD treatment led to an increase in parametrial/epididymal fat pad and elevated serum leptin levels in $Thrb^{PV/PV}Pten^{+/-}$ mice. Further molecular analyses indicated that the HFD induced more aggressive pathological changes that were mediated by increased activation of the Janus kinase 2-signaling transducer and activator of transcription 3 (STAT3) signaling pathway and induction of STAT3 target gene expression. Our findings demonstrate that diet-induced obesity exacerbates thyroid cancer progression in $Thrb^{PV/PV}Pten^{+/-}$ mice and suggest that the STAT3 signaling pathway could be tested as a potential target for the treatment of thyroid cancer. **(*Endocrinology* 154: 2936–2947, 2013)**

The incidence of thyroid cancer, the most common malignancy in the endocrine organs, has greatly increased worldwide in the past 2 decades (1). During the same period, the prevalence of obesity has doubled, and overweight in children and adolescents has tripled in the United States (2). Recent epidemiological studies provide strong evidence that obesity is an independent risk factor for thyroid cancer (3–6). A recent study also reported that high body mass index is strongly correlated with larger tumor size, extrathyroidal extension, and advanced stage of thyroid cancer (7). Still the molecular mechanisms by which obesity increases the risk of cancer are poorly understood. Animal models that can be interrogated during thyroid carcinogenesis would be a powerful approach to evaluate the impact of obesity on thyroid cancer development.

To this end, we took advantage of an animal model that spontaneously develops metastatic follicular thyroid cancer (FTC). This mouse harbors a knock-in dominant negative mutation, known as PV, in the *Thrb* gene locus (8). The PV mutation was identified in a patient suffering from resistance to thyroid hormone (9). As $Thrb^{PV/PV}$ mice age, their thyroids undergo pathological changes from hyperplasia to capsular and vascular invasion, anaplasia, and

ISSN Print 0013-7227 ISSN Online 1945-7170
Printed in U.S.A.

Received February 6, 2013. Accepted June 3, 2013.
First Published Online June 7, 2013

For editorial see page 2567

Abbreviations: AKT, protein kinase B; ATC, anaplastic thyroid cancer; DTC, differentiation thyroid cancer; FTC, follicular thyroid cancer; GAPDH, glyceraldehyde-3-phosphate dehydrogenase; H&E, hematoxylin-eosin; HFD, high-fat diet; IHC, immunohistochemistry; JAK, Janus kinase; LFD, low-fat diet; p, phosphorylated; PI3K, phosphatidylinositol 3-kinase; PV, knock-in dominant negative mutation; qRT-PCR, quantitative real-time RT-PCR; Rb, retinoblastoma; STAT, signaling transducer and activator of transcription.

eventual metastasis to the lung (10). The pathological progression, route, and frequency of metastasis in $Thrb^{PV/PV}$ mice are similar to that in human FTC. Extensive molecular analyses of altered signaling pathways during thyroid carcinogenesis have shown that the $Thrb^{PV/PV}$ mouse model faithfully recapitulates the molecular aberrations found in human thyroid cancer (11–15). To shorten the time in the spontaneous development of FTC, we have further introduced a haplodeficiency of the *Pten* gene (phosphatase and tensin homologue deleted from chromosome 10) into $Thrb^{PV/PV}$ mice ($Thrb^{PV/PV}Pten^{+/-}$ mice) (16). The loss of one allele of the tumor suppressor, the *Pten* gene, further exacerbates the overactivated phosphatidylinositol 3-kinase (PI3K)-protein kinase B (AKT) signaling in the thyroid tumors of $Thrb^{PV/PV}Pten^{+/-}$ mice, leading to reduced survival and faster cancer progression (11, 16). This aggressive thyroid cancer phenotype has provided a new opportunity for preclinical studies with the advantage of reaching the end point sooner. Indeed, the $Thrb^{PV/PV}Pten^{+/-}$ mice have been successfully used to test new kinase inhibitors for the treatment of thyroid cancer (17, 18). Thus, this spontaneous thyroid cancer model is ideal for assessing the effect of diet-induced obesity on thyroid cancer progression.

In the present study, we showed that the obesity induced by a high-fat diet (HFD) not only stimulated thyroid tumor growth but also promoted anaplastic change in the thyroid cancers of $Thrb^{PV/PV}Pten^{+/-}$ mice. Diet-induced obesity propelled thyroid tumor growth by increasing cell proliferation. Accompanying the increases in the parametrial/epididymal fat pad were markedly elevated serum leptin levels in $Thrb^{PV/PV}Pten^{+/-}$ mice. The elevated leptin was associated with the Janus kinase 2 (JAK)-signaling transducer and activator of transcription (STAT)-3 signaling pathway and STAT3 target gene expression, leading to promoting thyroid cancer progression. These findings indicate that obesity-induced metabolic change could account for more aggressive thyroid cancer and that the STAT3 signaling pathway is a potential therapeutic target for thyroid cancer exacerbated by obesity.

Materials and Methods

Animals and treatment

The National Cancer Institute Animal Care and Use Committee approved the protocols for animal care and handling in this study. Mice harboring the *ThrbPV* gene ($Thrb^{PV/PV}$ mice) were prepared via homologous recombination, and genotyping was carried out using the PCR method, as previously described (8). $Pten^{+/-}$ mice were kindly provided by Dr Ramon Parsons (Columbia University, New York, New York). $Thrb^{PV/PV}Pten^{+/-}$ mice were obtained by first crossing $Pten^{+/-}$ mice with $Thrb^{PV/+}$ mice and then crossing $Thrb^{PV/+}Pten^{+/-}$ with $Thrb^{PV/+}Pten^{+/+}$ mice. The control low-fat diet (LFD; 10% calories from fat) and the HFD (60% calories from fat) were purchased from Research Diets (New Brunswick, New Jersey). The mice were randomly selected and divided into 2 groups: LFD and HFD. The mice were fed these diets from the age of 6 weeks until the end of the study. The weight of the mice was measured every week, and the mice were monitored until they reached the age of 21 weeks or they became moribund with rapid weight loss, hunched posture, and labored breathing. When the mice were euthanized, blood was collected and the thyroids, lung, right inguinal fat, epididymal/parametrial fat, and liver tissues were dissected and weighted.

Histopathological analysis

Tissues from one lobe of the thyroid glands, lungs, epididymal/parametrial fat, and liver were fixed in 10% neutral-buffered formalin (Sigma-Aldrich, St Louis, Missouri) and subsequently embedded in paraffin. Five-micrometer-thick sections were prepared and stained with hematoxylin-eosin (H&E). For each animal we randomly selected and examined 3 sequential sections of tissues. The pathological evaluation of thyroid cancer progression was done as previously described (18).

Immunohistochemistry (IHC) was performed as previously described with some modification (12). Rabbit anti-Ki67 antibody (1:600 dilution; Neomarker, Thermo Scientific, Fremont, California), rabbit anti-phosphorylated (p)-Rb antibody (1:300 dilution; Cell Signaling, Danvers, Massachusetts), rabbit anti-cyclin D1 antibody (1:200, Neomarker), rabbit anti-p-STAT3 antibody (1:100 dilution; Cell Signaling), and rabbit anti-p-JAK2 antibody (1:50 dilution; Cell Signaling) were used for primary antibodies. The antigen signals were detected by treatment with the peroxidase substrate diaminobezidine followed by counterstaining with Gill's hematoxylin (Electron Microscopy Sciences, Hatfield, Pennsylvania). Relative cell density was quantified, and Ki-67-positive cells were evaluated in 8 thyroid sections from each group by using NIH Image software (Image J 1.34s; Wayne Rasband, National Institutes of Health, Bethesda, Maryland).

Western blot analysis

The protein extracts from thyroid tumors was prepared as previously described (19). The protein sample (20 μg) was loaded and separated by sodium dedecyl sulfated-polyacrylamide gel (Invitrogen, Carlsbad, California) electrophoresis. After electrophoresis, the protein was electrotransferred to a polyvinylidene difluoride membrane (Immobilon-P; Millipore Corp, Bedford, Massachusetts). The antibodies to p-Rb (1:500 dilution), total Rb (1:250 dilution), p-ERK (1:1000 dilution), total ERK (1:1000 dilution), p-AKT (1:1000 dilution), total AKT (1:1000 dilution), p-STAT3 (1:1000 dilution), total STAT3 (1:1000 dilution), p-JAK2 (1:1000 dilution), total JAK2 (1:1000 dilution), p-Rb (1:500 dilution), total Rb (1:250 dilution), and glyceraldehyde-3-phosphate dehydrogenase (GAPDH; 1:1000 dilution) were purchased from Cell Signaling Technology. Antibody for cyclin D1 (1:300 dilution) was purchased from Santa Cruz Biotechnology (Santa Cruz, California). The blots were stripped with Re-Blot Plus (Chemicon, Temecula, California) and reprobed with rabbit polyclonal antibody to GAPDH. Band intensities were quantified by using NIH Image software.

Hormone assay

Serum levels of TSH were measured as previously described (20). Serum levels of leptin and adiponectin of the mice were measured by commercialized (RIA) kits (catalog number ML-82K, and MADP-60HK) from Millipore Corp.

Quantitative real-time RT-PCR (qRT-PCR)

Total RNA from thyroid tumor tissues was isolated using TRIzol (Invitrogen), and this step was followed by ribonuclease-free deoxyribonuclease treatment and column purification according to the manufacturer's protocol (RNeasy minikit; QIAGEN, Valencia, California). For qRT-PCR, one-step RT-PCR reactions were performed with 200 ng of total RNA using a QuantiTect SYBR green RT-PCR kit (QIAGEN) in 7900HT Fast real-time PCR system (Applied Biosystems, Foster City, California) according to the manufacturer's instructions.

Acute treatment of wild-type mice with leptin

Recombinant leptin (Peprotech Tech, Rocky Hill, New Jersey; catalog number 300-027) was dissolved in PBS and 0.1% BSA buffer according to the manufacturer's instructions. Recombinant leptin (20 μg/mouse; 200 μl) was administrated ip. Mice were euthanized and thyroids were harvested after 30 and 60 min after injection of leptin.

Statistical analysis

Data are presented as mean ± SE, and a Student's *t* test was used to compare continuous variables. Two-way ANOVA was used to compare weekly weight gain between the 2 groups. A Fisher's exact test was used for comparison of categorical variables. The Kaplan-Meier method with log-rank test was used for comparison of survival in each group. *P* values were 2 sided throughout, and $P < .05$ was considered statistically significant. Data were analyzed using SPSS statistics version 19.0 (SPSS Inc, Chicago, Illinois). GraphPad PRISM 4.0a (GraphPad Software, San Diego, California) was used to draw graphs.

Results

High-fat diet-induced obesity exacerbates thyroid carcinogenesis of *Thrb*$^{PV/PV}$*Pten*$^{+/-}$ mice

Thrb$^{PV/PV}$*Pten*$^{+/-}$ mice were fed a HFD to induce obesity, beginning at 6 weeks of age. The weekly weight gain in the HFD group (females = 12 and males = 14) and LFD control group (females = 12 and males = 13) is shown in Figure 1A (females) and Figure 1B (males). Body weights of HFD group were significantly increasing pattern comparing with LFD control in both gender ($P < .001$). In the HFD group, the weekly weight gain was similar for both sexes. At the study end point, weight was significantly higher in the HFD than the LFD group ($P = .007$ in female mice and $P = .004$ in male mice; Figure 1C). The weights of the inguinal fat pads (sc fat) (Figure 2A) and the parametrial/epididymal fat pads (visceral fat) (Figure 2B) were clearly greater in both male and female mice fed an HFD than in those fed an LFD. Histological analysis by H&E staining of parametrial/epididymal fat pad further shows that the size of white adipocytes in HFD group (Figure 2C, panel b) was clearly increased as comparing with LFD control (Figure 2C, panel a). Figure 2D shows that the liver weight was also higher in the HFD mice than in the LFD controls. Histological analysis (H&E staining) showed that more lipids were present in the liver of HFD-fed mice (compare Figure 2E, panel b with panel a). Taken together, these data indicated that HFD treatment successfully induced obesity in *Thrb*$^{PV/PV}$*Pten*$^{+/-}$ mice.

To determine the effects of diet-induced obesity on thyroid carcinogenesis, we compared the survival of *Thrb*$^{PV/PV}$ *Pten*$^{+/-}$ mice fed an HFD with that of those fed an LFD. Mice became moribund with signs of palpable tumor, labored breathing, hunched position, and rapid weight loss due to the enlargement of thyroid tumors, as previously reported (16–18). The survival time of the HFD mice (n = 26) was significantly shorter than that of the LFD mice (n = 25, $P = .02$, Figure 3A). Only 11% in the HFD group survived to the study end point (21 wk), but 42% in the LFD group did so ($P = .02$). Thyroids from euthanized *Thrb*$^{PV/PV}$*Pten*$^{+/-}$ mice were dissected and weighed. As shown in Figure 3B, thyroid weights of HFD mice (n = 26) were significantly higher than those of LFD mice (n = 25, $P < .001$). There were no significant differences between

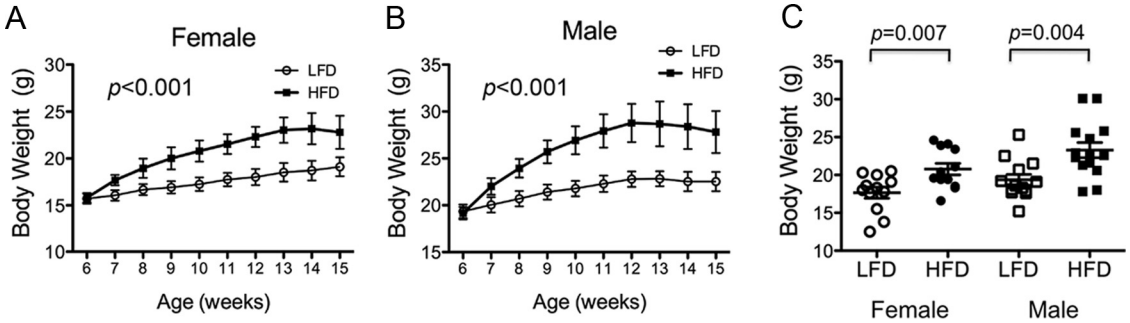

Figure 1. HFD induced weight gain in *Thrb*$^{PV/P}$*Pten*$^{+/-}$ mice. A, The difference in weekly weight gain of *Thrb*$^{PV/PV}$*Pten*$^{+/-}$ female mice after treatment with either a HFD (n = 12) or a LFD (n = 12). B, The difference in the weekly weight gain of *Thrb*$^{PV/PV}$*Pten*$^{+/-}$ male mice after treatment with either a HFD (n = 14) or a LFD (n = 13). Two-way ANOVA was used to compare the 2 groups. C, The body weight of *Thrb*$^{PV/PV}$*Pten*$^{+/-}$ mice at the study end point, according to their sex and diet.

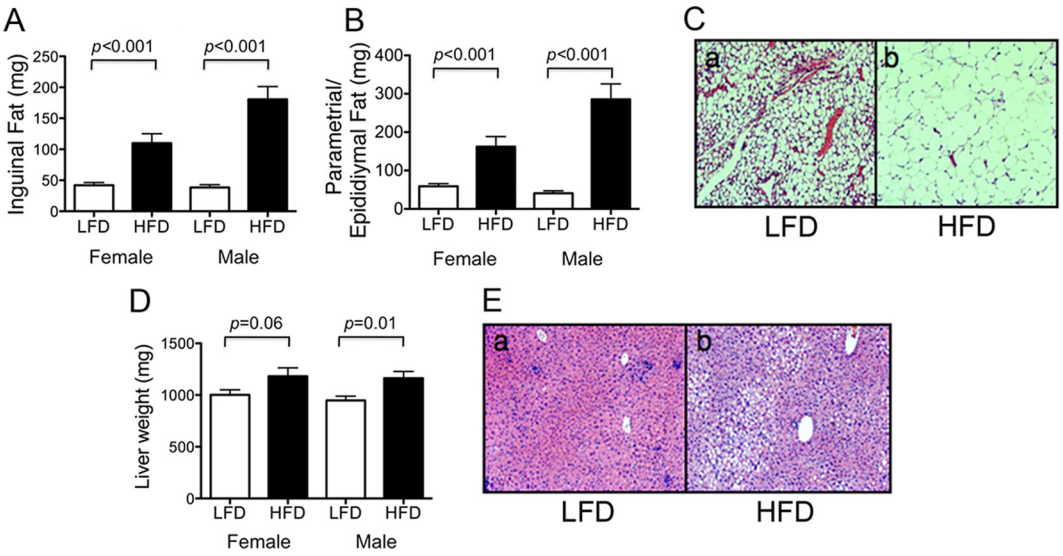

Figure 2. HFD induces obesity in *Thrb*$^{PV/PV}$*Pten*$^{+/-}$ mice. A, The weight of right inguinal fat (sc fat) of *Thrb*$^{PV/PV}$*Pten*$^{+/-}$ mice at the study end point, according to their sex and diet. B, The weight of parametrial fat (visceral fat) of female mice and epididymal fat of male mice at the study end point in the HFD (n = 26) and LFD (n = 25) groups. C, Representative microphotography of H&E staining on parametrial/epididymal fat tissue sections in the HFD and LFD groups. D, The liver weight of *Thrb*$^{PV/PV}$*Pten*$^{+/-}$ mice at the study end point, according to their sex and diet. The data, presented as mean ± SE, were analyzed by a Student's *t* test. E, Representative microphotography of H&E staining on liver tissue sections in the HFD and LFD groups.

male and female *Thrb*$^{PV/PV}$*Pten*$^{+/-}$ mice in survival and thyroid tumor size (data not shown). The differences in the size of thyroid tumors between the HFD and LFD groups were also apparent in formalin-fixed single lobes of thyroids (Figure 3C) and H&E-stained thyroid sections (Figure 3D). These data clearly indicated that diet-induced obesity stimulated the growth of thyroid tumors and substantially decreased survival time in *Thrb*$^{PV/PV}$*Pten*$^{+/-}$ mice fed an HFD.

We further investigated the effect of diet-induced obesity on thyroid cancer progression by comparing the pathological features of thyroid cancer in HFD mice (n = 26) and LFD mice (n = 25). As shown in Figure 3E, the thyroids of all *Thrb*$^{PV/PV}$*Pten*$^{+/-}$ mice underwent hyperplasia. All thyroid tumors in the HFD group developed capsular invasion, but only 88% of thyroid tumors in the LFD group did so ($P = .07$). There was no significant difference in vascular invasion between the 2 groups. But, importantly, 62% of thyroid cancers in the HFD group underwent anaplasia vs only 24% in the LFD group ($P = .01$). Histopathological examples of H&E-stained thyroid tumor sections of 4 HFD-treated *Thrb*$^{PV/PV}$*Pten*$^{+/-}$ mice are shown in Figure 3F, panels b, c, d, and e at low magnification. The foci were clearly apparent at low magnification as indicated by arrows, which, when examined at high magnification, show loss of glandular differentiation, often with spindle cell anaplasia (Figure 3F, corresponding panels, b′, c′, d′, and e′). An example of H&E-stained thyroid tumor section without apparent foci from the age-matched LFD-treated *Thrb*$^{PV/PV}$*Pten*$^{+/-}$ mice is also shown for comparison (Figure 3F, panels a and a′ with low magnification and high magnification, respectively). These data indicated that diet-induced obesity promotes the progression of thyroid cancer in *Thrb*$^{PV/PV}$*Pten*$^{+/-}$ mice.

Increased proliferation of thyroid tumor cells in HFD-induced obese *Thrb*$^{PV/PV}$*Pten*$^{+/-}$ mice

To understand how HFD-induced obesity increased thyroid tumor growth, we examined cell proliferation by staining tumor cells with nuclear proliferation marker, Ki-67, in the thyroid sections of the LFD (Figure 4A, panels a and b) and HFD groups (Figure 4A, panels c and d). Cells stained with Ki-67 were counted and quantitative data are shown in Figure 4B, indicating approximately 35% more cells were positively stained with Ki-67 in the HFD group than in the LFD group ($P = .001$; n = 8 in each group). The cell numbers in the same area of thyroid sections of both groups of mice were counted, and the quantitative analysis showed a 64% higher cell density in the thyroid of the HFD group than in the LFD group (n = 8 in each group, Figure 4B, panel b, $P = .004$). These data indicated that the proliferation of tumor cells was stimulated in mice fed an HFD.

To understand how thyroid tumor cells increased cell proliferation in obese *Thrb*$^{PV/PV}$*Pten*$^{+/-}$ mice, we evaluated the abundance and activity of key regulators in the cell cycle progression of thyroid tumors. The level of phosphorylation of the retinoblastoma (Rb) was significantly

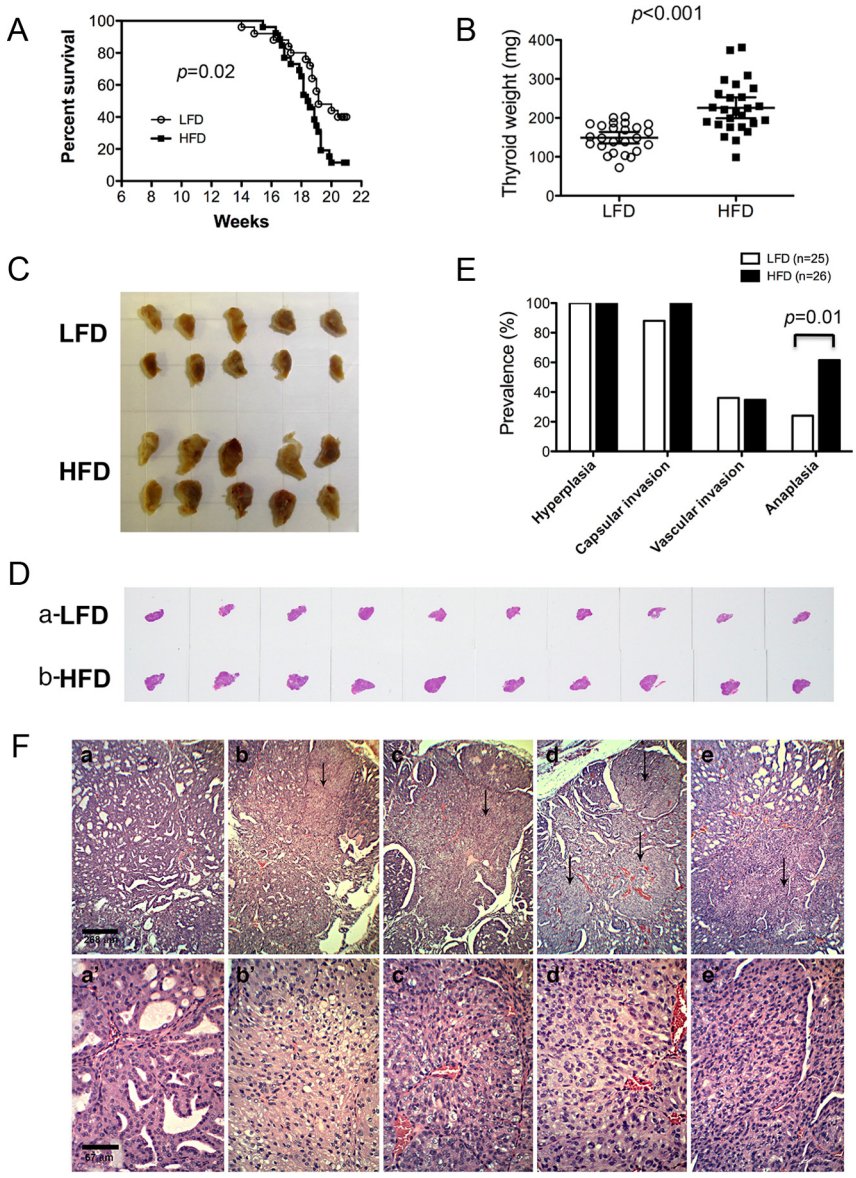

Figure 3. HFD-induced obesity exacerbates thyroid carcinogenesis in *Thrb*$^{PV/PV}$*Pten*$^{+/-}$ mice. A, The survival of *Thrb*$^{PV/PV}$*Pten*$^{+/-}$ mice was lower in the HFD group than the LFD group. The survival curves of each group were drawn by the Kaplan-Meier method, and the difference in survival was analyzed by the log-rank test. B, The thyroid tumor size in the HFD group (n = 26) was significantly larger than in the LFD group (n = 25). The weights of thyroid tumors from *Thrb*$^{PV/PV}$*Pten*$^{+/-}$ mice, presented as mean ± SE, were analyzed by a Student's *t* test. C, Representative pictures of thyroid tumors from *Thrb*$^{PV/PV}$*Pten*$^{+/-}$ mice, according to their diet. One lobe of thyroid was kept in 70% ethanol after fixation in 10% neutral buffered formalin. D, Gross pictures of H&E-stained tissue sections from thyroid tumors in the HFD (n = 10) and LFD (n = 10) groups. E, Pathological analysis of thyroid cancer progression in the LFD (n = 25) and HFD (n = 26) groups of *Thrb*$^{PV/PV}$*Pten*$^{+/-}$ mice. The frequency of each pathological feature in thyroid carcinogenesis, according to the diet, was represented by percentage and analyzed by a Fisher's exact test. F, Promoting anaplastic thyroid tumors by HFD in *Thrb*$^{PV/PV}$*Pten*$^{+/-}$ mice. H&E-stained thyroid tumor sections of LFD-treated *Thrb*$^{PV/PV}$*Pten*$^{+/-}$ mice are shown in panels a and a' at low magnification and high magnification, respectively. H&E-stained thyroid tumor sections of HFD-treated *Thrb*$^{PV/PV}$*Pten*$^{+/-}$ mice are shown in panels b, c, d, and e and b', c' d', and e' at low and high magnification, respectively. Representative samples of anaplastic loci indicated by arrows are apparent at low magnification in panels b, c, d, and e (×20). The foci are selected shown at high magnification in the corresponding panels b', c', d', and e', ×80).

increased in HFD mice (Figure 4C, panel a) without apparent changes in the total Rb level (Figure 4C, panel b). The increased protein level of p-Rb indicates an activated cell cycle progression because unphosphorylated Rb acts as a negative regulator of the G1-S cell cycle progression by binding to and inhibiting E2F family transcriptional factors in the G1-S transition. Consistently, Western blot analysis further showed that the protein levels of cyclin D1 were higher in the HFD group than the LFD group (Figure 4C, panel c). Figure 4C, panel d, shows the loading control using GAPDH.

The increased protein abundance of p-Rb and cyclin D1 detected by Western blot was further confirmed by IHC analysis. Figure 4D, panels b and d, shows that nuclear staining by anti-p-Rb [p-Rb (S807/810)] and cyclin D1, respectively, was stronger in thyroid tumor cells of obese *Thrb*$^{PV/PV}$*Pten*$^{+/-}$ mice than in controls (Figure 4D, panels a and c). These data indicate that thyroid tumor cells of obese *Thrb*$^{PV/PV}$ *Pten*$^{+/-}$ mice exhibited higher cell proliferation, resulting in increased tumor growth.

Previously we reported that the pituitary-thyroid axis is dysregulated with elevated levels of serum TSH in *Thrb*$^{PV/PV}$*Pten*$^{+/-}$ mice (16). Because TSH is an important stimulator of thyroid cell proliferation, we further evaluated whether the TSH serum level was altered by an HFD to affect proliferation of thyroid tumor cells in HFD-treated *Thrb*$^{PV/PV}$ *Pten*$^{+/-}$ mice. As shown in Figure 4E, there was no significant difference in serum TSH levels between the 2 groups, indicating that HFD treatment did not affect the TSH levels of *Thrb*$^{PV/PV}$*Pten*$^{+/-}$ mice. Thus, the increased thyroid tumor size and anaplastic change in the HFD group was not mediated by the change in serum TSH levels.

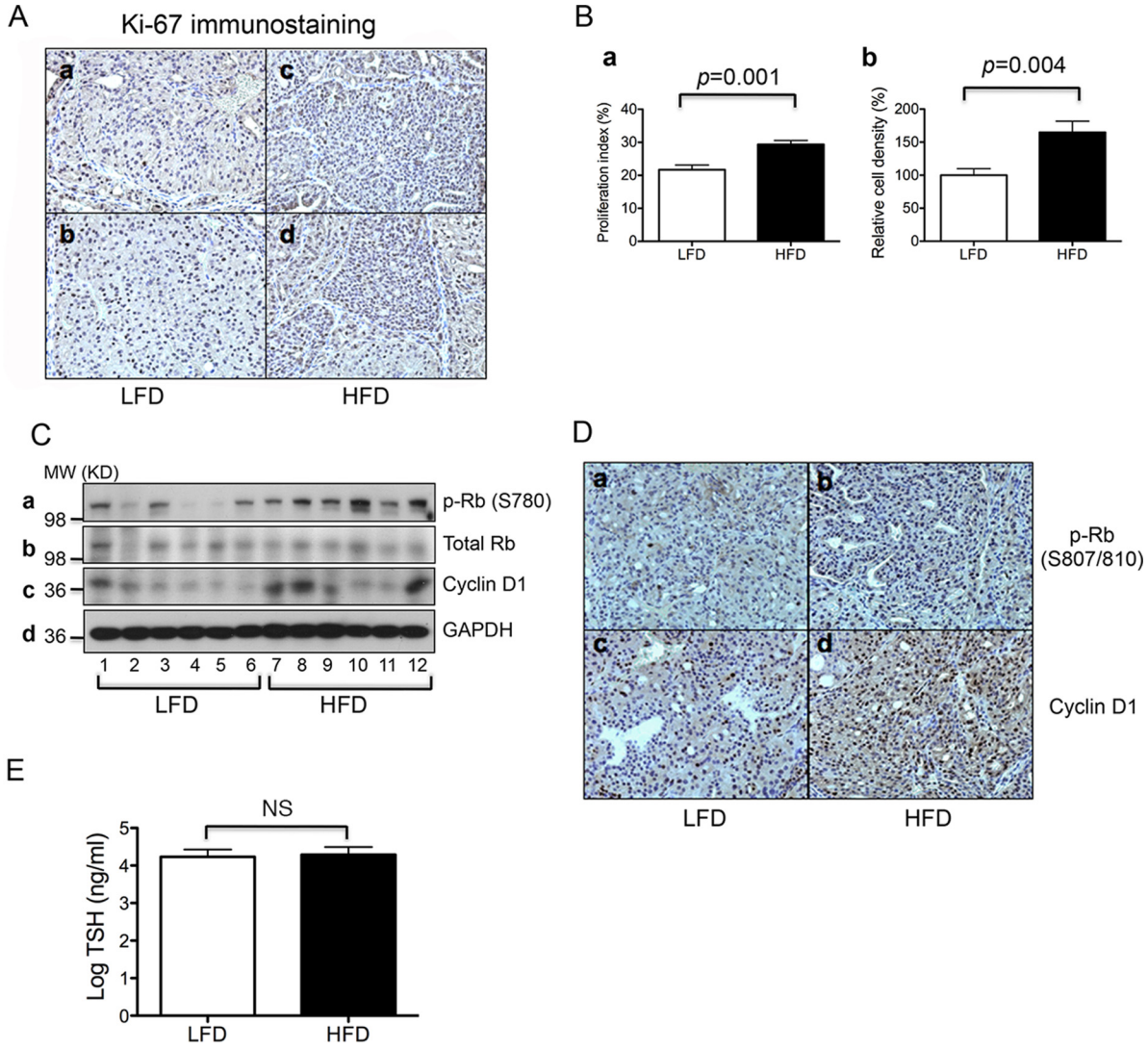

Figure 4. HFD induces thyroid cancer cell proliferation in *Thrb*$^{PV/PV}$*Pten*$^{+/-}$ mice. A, Representative microphotographs of Ki-67 IHC on thyroid sections of the LFD group (a and b) and HFD group (c and d). B, Thyroid cancer cell proliferation index, determined by Ki-67-positive cells in the HFD and LFD groups (B, panel a). The relative cell density was determined by quantification of cell number in the high-power field in the 2 groups (B, panel b). The number of thyroid tumor sections was 8 for each group. Data, presented as mean ± SE, were analyzed by a Student's *t* test. C, Western blot analysis of phosphorylated Rb (S780), total Rb, cyclin D1, and GAPDH as a loading control in the HFD (n = 6) and LFD (n = 6) groups. D, Representative microphotographs of p-Rb (S807/810) and cyclin D1 IHC on thyroid tumor sections from the LFD (D, panels a and c) and HFD (D, panels b and d) groups. E, Comparison of serum TSH levels of *Thrb*$^{PV/PV}$*Pten*$^{+/-}$ mice treated with an HFD (n = 24) or LFD (n = 24). Data, presented as mean ± SE of log TSH, were analyzed by a Student's *t* test.

Activation of JAK2-STAT3 signaling by diet-induced obesity in the thyroid cancer in *Thrb*$^{PV/PV}$ *Pten*$^{+/-}$ mice

We further sought to understand the mechanisms by which HFD-induced obesity promotes thyroid carcinogenesis in *Thrb*$^{PV/PV}$*Pten*$^{+/-}$ mice. Extensive studies have shown that adipose tissue secretes adipokines, such as leptin and adiponectin, into blood circulating systems to signal other metabolic organs or the brain to coordinate responses to altered metabolic demands. Leptin is an adiocyte-derived hormone that is the central regulatory mediator of appetite and energy homeostasis (21). Leptin levels are closely correlated with adiposity in humans and rodents (22) and may be linked to an increased incidence of cancer in obesity (23). Adiponectin, a regulator of glucose and lipid metabolism, may have antitumor effects, given that its levels are reduced in obesity (23, 24). Because we found that *Thrb*$^{PV/PV}$*Pten*$^{+/-}$ mice fed an HFD had increased fat pads with enlarged adipocytes (Figure 2, A–C), we examined the serum levels of leptin and adiponectin of wild-type and *Thrb*$^{PV/PV}$*Pten*$^{+/-}$ mice. As shown in Figure 5A, panel a, wild-type mice treated with HFD had higher serum leptin levels than those treated with LFD (Figure 5A, panel a, compare data group 2 with 1). Similarly, higher serum leptin levels were detected for *Thrb*$^{PV/PV}$*Pten*$^{+/-}$ mice treated with HFD than those

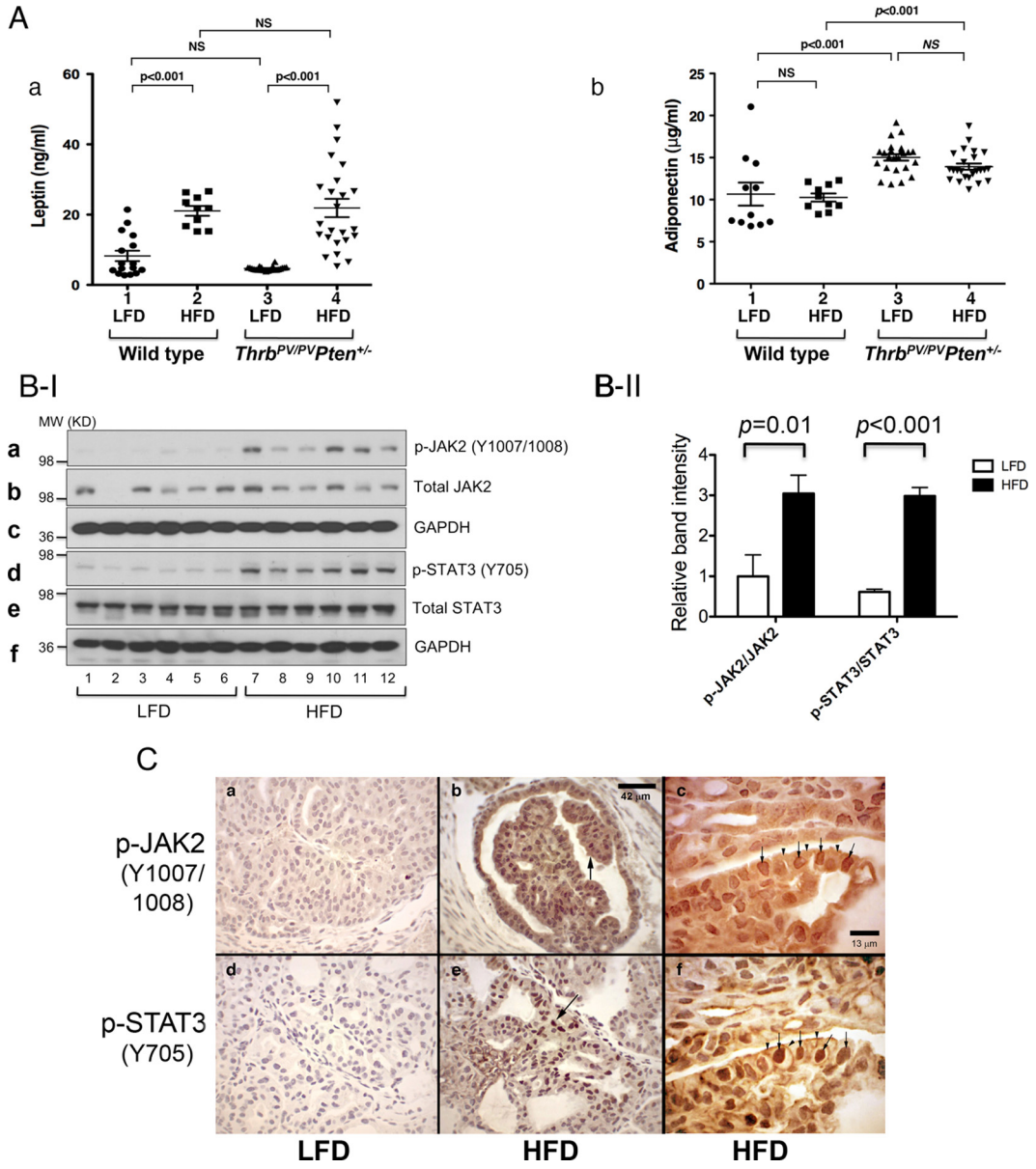

Figure 5. Altered serum adipokine levels and activated JAK and STAT signaling in thyroid carcinogenesis of obese *Thrb*$^{PV/PV}$*Pten*$^{+/-}$mice. Effects of diet on serum leptin concentrations (A, panel a) and adiponectin concentrations in wild-type and *Thrb*$^{PV/PV}$*Pten*$^{+/-}$ mice (A, panel b) are shown. The serum leptin and adiponectin concentrations from wild-type mice treated with LFD (n = 11) or with HFD (n = 10) were determined as described in *Materials and Methods*. Serum leptin and adiponectin concentrations from *Thrb*$^{PV/PV}$*Pten*$^{+/-}$ mice treated with LFD (n = 24) or with HFD (n = 24) were also determined. The *P* values are indicated. B, panel I, Western blot analysis of p-JAK2 (Y1007/1008), total JAK2, p-STAT3 (Y705), total STAT3, and GAPDH as a loading control in the HFD (n = 6) and LFD (n = 6) groups. B, panel II, Quantification of relative ratio of protein abundance of p-JAK2/total JAK2 and p-STAT3/total STAT3 after normalization. Data, presented a mean ± SE, were analyzed by a Student's *t* test. C, Comparison between the 2 groups of representative microphotographs of IHC using anti-p-JAK2 (panels a, b, and c) and anti-p-STAT3 (panels d, e, and f) antibody on thyroid sections. The magnification of images in panels a, b, d, and e is ×100; in panels c and f is ×250. D, Recombinant leptin activates STAT3 in the wild-type mice thyroid. D, panel I, Representative microphotographs of p-STAT3 IHC on thyroid sections of wild-type mice without (a and b) or with recombinant leptin treatment (panels c, d, e, and f) for 30 minutes (panels c and d) or for 60 minutes (panels e and f). The arrows indicate the positively stained cells. The negative without the treatment with primary antibodies are shown in the corresponding panels a, c, and e. D, panel II, The p-STAT3-positive cells were counted and the data are expressed as a percentage of p-STAT3-positive cells vs total cells. The data are expressed as mean ±SE (n = 2–4 slides). The *P* values are shown. E, Western blot analysis of p-AKT, total AKT, p-ERK1/2, total ERK1/2, and GAPDH as a loading control in the HFD (n = 6) and LFD (n = 6) groups.

treated with LFD (Figure 5A, panel a, compare data group 4 with group 3). No significant differences in the serum leptin levels were observed between wild-type mice and *Thrb*$^{PV/PV}$*Pten*$^{+/-}$ mice treated with LFD (Figure 5A, panel a, compare data group 3 with group 1) and between wild-type mice and *Thrb*$^{PV/PV}$*Pten*$^{+/-}$ mice treated with HFD (Figure 5A, panel a, compare data group 4 with group 2). These data indicate that the extent of the increase

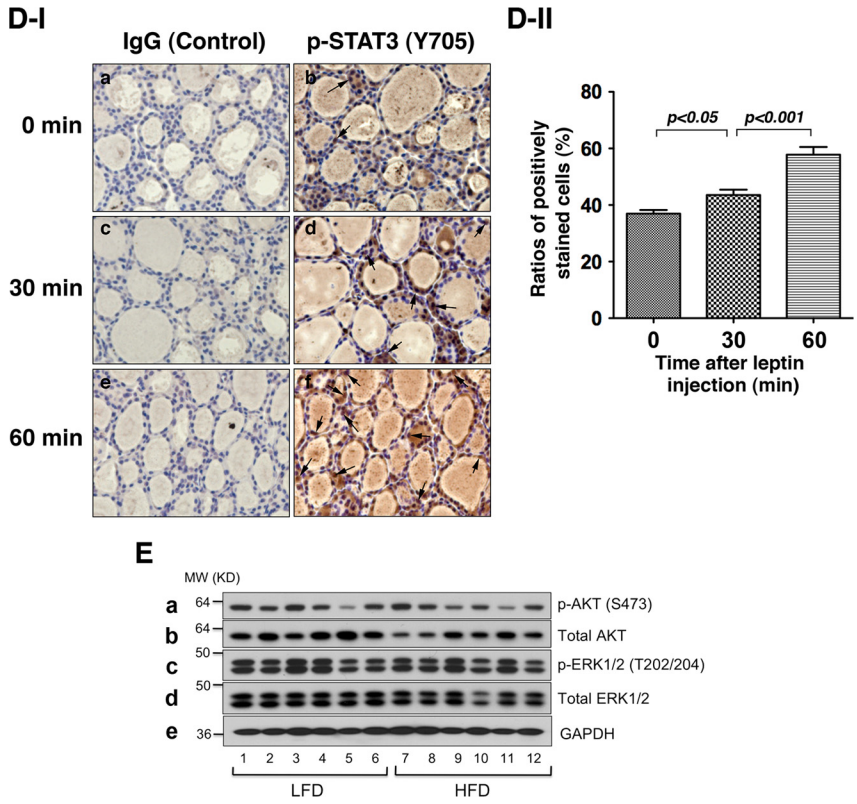

Figure 5. (Continued)

in serum leptin levels by HFD is virtually equal in wild-type and $Thrb^{PV/PV}Pten^{+/-}$ mice and is not disproportionally different between wild-type and $Thrb^{PV/PV}Pten^{+/-}$ mice.

As shown in Figure 5A, panel b, serum adiponectin levels of wild-type mice treated with HFD, although they had a small trend to edge lower, were not significantly different from those treated with LFD (Figure 5A, panel b, compare data group 2 with group 1). Interestingly, serum adiponectin levels were higher in LFD-treated $Thrb^{PV/PV}Pten^{+/-}$ mice than in LFD-treated wild-type mice (Figure 5A, panel b, compare data group 3 with group 1). However, serum adiponectin levels of the $Thrb^{PV/PV}Pten^{+/-}$ mice were not significantly affected by HFD treatment (Figure 5A, panel b, compare data group 4 with group 3). These results suggest that adiponectin most likely did not play a significant role in the HFD-exacerbated thyroid carcinogenesis.

STAT3, a transcriptional factor activated by cytokines and growth factors, plays a critical role in cell survival, proliferation, and differentiation (25). In genetic and dietary models of obesity, the activation of STAT3 is increased in tumors grown in obese animals (26). Interestingly, circulating leptin produced from adipose tissues can activate the JAK2-STAT3 signaling pathway (5, 25). The increased leptin levels we found (Figure 5A, panel a) prompted us to assess the activity of the JAK2-STAT3 signaling pathway in obese $Thrb^{PV/PV}Pten^{+/-}$ mice to understand its impact on thyroid carcinogenesis. The protein levels of p-JAK2 (Tyr 1007/1008) were significantly higher in thyroid tumors from HFD than from LFD mice (Figure 5, B-I, panel a). But the total JAK2 was not affected by the diet (Figure 5 B-I, panel b). The p-STAT3 (Tyr 705) levels, critical for the activity of downstream signaling, were higher in thyroid tumors of HFD than LFD mice without any change in total STAT3 protein levels between the 2 groups (Figure 5, B-I, panel d). The intensities of the bands in Figure 5, B-I, were determined, and the quantitative comparison is shown in Figure 5, B-II.

The activation of the JAK2-STAT3 signaling pathway was also confirmed by IHC. The staining signals of p-JAK2 (Y1007/1008) and p-STAT3 (Y705) were visible with higher intensity in thyroid tumor sections from HFD mice (Figure 5C, panels b and c, and d and f) than staining signals from LFD controls (Figure 5C, panels a and d). The nuclear signals of p-JAK2 and p-STAT3 indicated by arrows were clearly visible in Figure 5C, panels c and f, respectively, that had higher magnification than in Figure 5C, panels b and e. The arrowheads show the cytoplasmic/plasma membrane localization of p-JAK2 and p-STAT3 (Figure 5C, panels e and f, respectively). These data indicate that the JAK2-STAT3 signaling cascades were important effectors on thyroid cancer growth and progression in diet-induced obese $Thrb^{PV/PV}Pten^{+/-}$ mice.

That STAT signaling could be activated by the elevated leptin in the thyroid and was demonstrated by acute treatment of wild-type mice with leptin. As shown in Figure 5D-I, immunostaining of p-STAT was visibly higher than the basal signals without leptin treatment in the thyroid follicular cells 30 minutes after the ip injection of leptin (indicated by arrows; Figure 5D-I, panel d, vs 5D-I, panel b). More p-STAT positively stained follicular cells were apparent after treatment of mice with leptin for 60 minutes (Figure 5D-I, panel f). The negative controls were shown in Figure 5D-I, panels a, c, and e, respectively, at 0 time and 30 and 60 minutes after leptin treatment. These results demonstrate that the acute systematic leptin treatment activated the STAT signaling in the thyroid in vivo.

Previously we showed that the activation of PI3K-AKT signaling promotes thyroid carcinogenesis of $Thrb^{PV/PV}$ $Pten^{+/-}$ mice (16, 19). It is known that obesity increases insulin and IGF signals, leading to the downstream activation of PI3K-AKT signaling (23). We therefore examined whether there were changes in PI3K-AKT signaling in the thyroid tumors of HFD-fed $Thrb^{PV/PV}Pten^{+/-}$ mice. As shown in Figure 5E, panel a, of no significant difference in the protein abundance of p-AKT was found between the HFD and LFD groups. MAPK is important for the response to extracellular stimuli to affect cell proliferation, survival, and differentiation (27). We also questioned whether there were changes in the MAPK signaling pathway that could affect thyroid carcinogenesis in obese $Thrb^{PV/PV}Pten^{+/-}$ mice. To this end, we analyzed the protein abundance of p-ERK1/2 and total ERK1/2, which are the downstream effectors of the MAPK signaling pathway. No significant differences in protein levels of p-ERK1/2 and total ERK1/2 were detected (Figure 5E, panels c and d). Figure 5E, panel e, is the loading control using GAPDH. These results indicated that PI3K-AKT and MAPK signaling did not contribute to the more aggressive thyroid carcinogenesis observed in diet-induced obese $Thrb^{PV/PV}Pten^{+/-}$ mice.

Activated expression of STAT3 target genes in thyroid tumors of obese $Thrb^{PV/PV}Pten^{+/-}$ mice

To evaluate further the functional consequences of the activation of the JAK2-STAT3 signaling pathway in HFD mice, we used qRT-PCR to compare the expression of STAT3 target genes in thyroid tumors from this group (n = 14) and the LFD group (n = 14). The *Socs3* (suppressor of cytokine signaling 3) gene, induced by cytokines and leptin, is a negative regulator of the JAK2-STAT3 signaling pathway. Figure 6 shows that the mRNA expression level of *Socs3* was 2.9-fold higher in the HFD group than in the LFD group ($P < .001$, Figure 6, panel a). *Mcl1* and *Vegfa* are critical STAT3 target genes to mediate

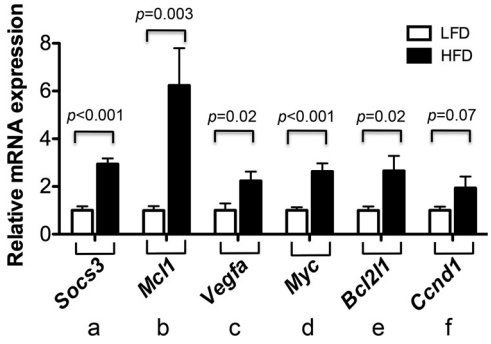

Figure 6. HFD induces the expression of STAT3 target genes in thyroid tumors of $Thrb^{PV/PV}Pten^{+/-}$ mice. The relative mRNA expression of *Socs3* (a), *Mcl1* (b), *Myc* (c), *Vegfa* (d), *Bcl2l1* (e), and *Ccnd1* (f) in thyroid tumors from the HFD (n = 14) and LFD (n = 14) groups. The data, presented mean ± SE, were analyzed by a Student's *t* test.

the actions of STAT3 in human cancer (28). HFD significantly induced the mRNA expression of these 2 genes by 6.2-fold ($P = .003$, Figure 6, panel b) and 2.2 -fold ($P = .02$, Figure 6, panel c), respectively, as compared with the LFD group. We also evaluated the expression of *Myc*, *Bcl2l1*, and *Ccnd1*, identified as STAT3 target genes, to promote STAT3-mediated cancer cell migration and invasion (29). The mRNA expression levels of these genes in thyroid tumor tissues were higher in HFD $Thrb^{PV/PV}$ $Pten^{+/-}$ mice than in LFD controls (Figure 6, panels d–f). These results indicated that the activation of the JAK2-STAT3 signaling pathway was critical for the development of the more aggressive thyroid cancer induced by HFD in $Thrb^{PV/PV}Pten^{+/-}$ mice.

Discussion

Using the spontaneously developed thyroid cancer mouse model, $Thrb^{PV/PV}Pten^{+/-}$ mice, we evaluated the effects of diet-induced obesity on thyroid carcinogenesis from tumor development to anaplastic change. Feeding $Thrb^{PV/PV}$ $Pten^{+/-}$ mice an HFD for 15 weeks successfully induced the phenotype of obesity in our mouse model. Even though there was no significant change in the early development stages of thyroid cancer such as hyperplasia and capsular invasion, the HFD clearly increased thyroid tumor growth and induced a more aggressive phenotype with anaplastic change of thyroid carcinoma. To our knowledge, this is the first study showing the detrimental role of diet-induced obesity in thyroid carcinogenesis using a mouse model.

Patients with anaplastic thyroid cancer (ATC) and dedifferentiated thyroid cancer are usually resistant to current treatment and have a very poor prognosis. Although there are ongoing research efforts, the detailed mechanisms by which the dedifferentiation process occurs are still unclear. ATC is one of the most aggressive types of malig-

nancy in humans (30). It is generally accepted that ATC usually develops by transformation or dedifferentiation of preexisting differentiation thyroid cancer (DTC). Previous studies reported that about 35%–71% of ATC coexisted with simultaneous DTC (30–32). The *Thrb*$^{PV/PV}$*Pten*$^{+/-}$ mouse should be very useful to evaluate the mechanisms of transformation or dedifferentiation because anaplastic foci of thyroid cancer coexist concurrently with follicular thyroid cancer and the occurrence of anaplastic foci increases in older mice, similar to human cancer (16). Importantly, the present study showed that the anaplastic change from DTC was significantly greater in HFD mice than LFD controls. In the present studies, we showed the activation of the JAK2-STAT3 signaling pathway (Figure 5, B and C) in HFD mice was associated with a higher occurrence of anaplastic foci (Figure 3E). These observations suggested that the activated JAK2-STAT3 signaling pathway could be a possible mechanism to mediate transformation or dedifferentiation of thyroid tumor cells.

The STAT proteins mediate various cellular and biological responses to cytokines and growth factors. Recruitment via the Src homology 2 domain to receptor phosphotyrosine peptide motifs facilitates STAT phosphorylation on a key tyrosyl residue by growth factor receptors and the JAK (25). The activated phosphorylation induces STAT-STAT dimerization and nuclear translocation and eventually by binding to specific DNA-response elements in the promoters of target genes activates gene transcription (29). The aberrant activation of STAT3 has been reported to promote cancer progression in many human cancers (25). Our study revealed that the obesity-induced thyroid tumor growth and cancer progression were mediated by the activated phosphorylation of oncogenic JAK2 and STAT3 transcription factors. These findings raised the possibility that STAT3 could be tested as a therapeutic target in thyroid cancer. Consistent with this notion, various kinds of STAT3 inhibitors are currently in the preclinical development stage (29, 33).

Our results showed that the serum leptin level was markedly elevated in HFD-induced obese *Thrb*$^{PV/PV}$ *Pten*$^{+/-}$ mice. The high leptin level was also closely correlated with adiposity of HFD *Thrb*$^{PV/PV}$*Pten*$^{+/-}$ mice (see Figure 2, A–C, and Figure 5 A, panel a). Obesity disrupts the functions of adipocytes in energy homeostasis, resulting in inflammation and alteration of adipokine signaling, which were recently shown to be important mediators in cancer development (23, 34). The expression of leptin in human thyroid cancer is also associated with thyroid cancer aggressiveness, including tumor size and lymph node metastasis (35), and leptin enhances migration of thyroid cancer cells (36). Importantly, leptin signals are known to mediate downstream signaling via the JAK2-STAT3 pathway (23). The present findings that elevated leptin levels were associated with activated JAK2-STAT3 signaling pathway, leading to more aggressive thyroid cancer of obese *Thrb*$^{PV/PV}$*Pten*$^{+/-}$ mice. However, it is of interest to point out that activation of JAK2-STAT3 by other cytokines such as IL-6 was also reported for gastric carcinoma (37) and colon cancer (38, 39). At present, it is unknown whether other cytokines (eg, IL-6) were altered during thyroid carcinogenesis of HFD-treated *Thrb*$^{PV/PV}$*Pten*$^{+/-}$ mice. Whether IL-6 and other yet-to-be-discovered cytokines also participated in the activation of JAK2-STAT3 would await future studies.

We also considered the possibility that the obesity induced by HFD in *Thrb*$^{PV/PV}$*Pten*$^{+/-}$ mice could also affect insulin and IGF signaling. It is known that in humans, obesity can lead to an elevated level of circulating insulin. Activation of insulin and IGF receptors results in the phosphorylation of the insulin receptor substrate proteins, which activates the oncogenic RAS-MAPK and PI3K-AKT signaling pathways (23). In our previous studies, we have shown the activation of multiple signaling pathways including PI3K-AKT and MAPK signaling in thyroid carcinogenesis of *Thrb*$^{PV/PV}$*Pten*$^{+/-}$ mice without HFD treatment (18). We therefore assessed whether HFD-induced obesity could affect PI3K-AKT and MAPK signaling in thyroid carcinogenesis of *Thrb*$^{PV/PV}$*Pten*$^{+/-}$ mice. Accordingly, we evaluated the protein abundance of p-ERK1/2 and p-AKT in thyroid tumors from HFD and LFD groups because these signaling pathways are critical for the development of human thyroid cancers. However, there were no significant differences between the 2 groups in the activation of the MAPK and PI3K signaling pathways (see Figure 5E).

The finding that the MAPK and PI3K signaling pathways were not affected during thyroid carcinogenesis of obese *Thrb*$^{PV/PV}$*Pten*$^{+/-}$ mice is highly significant in that these mice offer an advantage over other mouse models in studying the effects of obesity on carcinogenesis. Dissecting molecular mechanisms of obesity-induced carcinogenesis is frequently a challenge because complex arrays of multiple signaling pathways concurrently drive the oncogenic process. It is difficult to identify the sequential events and map out the networks. Finding that the MAPK and PI3K signaling pathways did not contribute to the more aggressive cancer phenotype of obese *Thrb*$^{PV/PV}$*Pten*$^{+/-}$ mice has provided us a unique opportunity to narrow our focus to the role of the JAK2-STAT3 signaling pathway in the dedifferentiation process of thyroid carcinogenesis. Moreover, our *Thrb*$^{PV/PV}$*Pten*$^{+/-}$ mouse model will be useful for preclinical studies evaluating the effects of JAK2 inhibitors, STAT3 inhibitors, and other antiobesity agents on thyroid carcinogenesis.

The present study has provided direct evidence of the detrimental effects of obesity on thyroid tumor size and anaplastic change in thyroid cancer in an animal model. HFD-induced obesity increased thyroid tumor growth by stimulating cancer cell proliferation and induced a more aggressive type of thyroid cancer in $Thrb^{PV/PV}Pten^{+/-}$ mice. These findings suggest that the current and potential therapeutic approaches for the treatment of obesity and related disease could be potential therapeutic options for the prevention and treatment of thyroid cancer. They also reinforce the importance of efforts aimed at early prevention of obesity, especially in children and adolescents, because these preventive approaches could provide the additional benefit of reducing thyroid cancer incidence and the social-economic costs associated with the diagnosis and treatment of thyroid cancer.

Acknowledgments

Intramural Research Program of the National Institutes of Health, National Cancer Institute, Center for Cancer Research. We thank Li Zhao for the technical assistance in the immunohistochemistry of p-STAT in the thyroid after acute treatment of leptin.

Address all correspondence and requests for reprints to: Sheueyann Cheng, PhD, Laboratory of Molecular Biology, National Cancer Institute, 37 Convent Drive, Room 5128, Bethesda, Maryland 20892-4264. E-mail: chengs@mail.nih.gov.

Disclosure Summary: The authors declare no conflict of interest.

References

1. **Kilfoy BA, Zheng T, Holford TR, et al.** International patterns and trends in thyroid cancer incidence, 1973–2002. *Cancer Causes Control*. 2009;20:525–531.
2. **Ogden CL, Yanovski SZ, Carroll MD, Flegal KM.** The epidemiology of obesity. *Gastroenterology*. 2007;132:2087–2102.
3. **Renehan AG, Tyson M, Egger M, Heller RF, Zwahlen M.** Body-mass index and incidence of cancer: a systematic review and meta-analysis of prospective observational studies. *Lancet*. 2008;371:569–578.
4. **Meinhold CL, Ron E, Schonfeld SJ, et al.** Nonradiation risk factors for thyroid cancer in the US Radiologic Technologists Study. *Am J Epidemiol*. 2010;171:242–252.
5. **Kitahara CM, Platz EA, Freeman LE, et al.** Obesity and thyroid cancer risk among US men and women: a pooled analysis of five prospective studies. *Cancer Epidemiol Biomarkers Prev*. 2011;20:464–472.
6. **Aschebrook-Kilfoy B, Sabra MM, Brenner A, et al.** Diabetes and thyroid cancer risk in the National Institutes of Health-AARP Diet and Health Study. *Thyroid*. 2011;21:957–963.
7. **Kim HJ, Kim NK, Choi JH, et al.** Associations between body mass index and clinico-pathological characteristics of papillary thyroid cancer. *Clin Endocrinol (Oxf)*. 2013;78(1):134–140.
8. **Kaneshige M, Kaneshige K, Zhu X, et al.** Mice with a targeted mutation in the thyroid hormone beta receptor gene exhibit impaired growth and resistance to thyroid hormone. *Proc Natl Acad Sci USA*. 2000;97:13209–13214.
9. **Parrilla R, Mixson AJ, McPherson JA, McClaskey JH, Weintraub BD.** Characterization of seven novel mutations of the c-erbA β gene in unrelated kindreds with generalized thyroid hormone resistance. Evidence for two "hot spot" regions of the ligand binding domain. *J Clin Invest*. 1991;88:2123–2130.
10. **Suzuki H, Willingham MC, Cheng SY.** Mice with a mutation in the thyroid hormone receptor β gene spontaneously develop thyroid carcinoma: a mouse model of thyroid carcinogenesis. *Thyroid*. 2002;12:963–969.
11. **Furuya F, Hanover JA, Cheng SY.** Activation of phosphatidylinositol 3-kinase signaling by a mutant thyroid hormone beta receptor. *Proc Natl Acad Sci USA*. 2006;103:1780–1785.
12. **Lu C, Zhao L, Ying H, Willingham MC, Cheng SY.** Growth activation alone is not sufficient to cause metastatic thyroid cancer in a mouse model of follicular thyroid carcinoma. *Endocrinology*. 2010;151:1929–1939.
13. **Ying H, Furuya F, Zhao L, et al.** Aberrant accumulation of PTTG1 induced by a mutated thyroid hormone beta receptor inhibits mitotic progression. *J Clin Invest*. 2006;116:2972–2984.
14. **Kim CS, Ying H, Willingham MC, Cheng SY.** The pituitary tumor-transforming gene promotes angiogenesis in a mouse model of follicular thyroid cancer. *Carcinogenesis*. 2007;28:932–939.
15. **Guigon CJ, Zhao L, Lu C, Willingham MC, Cheng SY.** Regulation of β-catenin by a novel nongenomic action of thyroid hormone beta receptor. *Mol Cell Biol*. 2008;28:4598–4608.
16. **Guigon CJ, Zhao L, Willingham MC, Cheng SY.** PTEN deficiency accelerates tumour progression in a mouse model of thyroid cancer. *Oncogene*. 2009;28:509–517.
17. **Guigon CJ, Fozzatti L, Lu C, Willingham MC, Cheng SY.** Inhibition of mTORC1 signaling reduces tumor growth but does not prevent cancer progression in a mouse model of thyroid cancer. *Carcinogenesis*. 2010;31:1284–1291.
18. **Kim WG, Guigon CJ, Fozzatti L, et al.** SKI-606, an Src inhibitor, reduces tumor growth, invasion, and distant metastasis in a mouse model of thyroid cancer. *Clin Cancer Res*. 2012;18:1281–1290.
19. **Kim CS, Vasko VV, Kato Y, et al.** AKT activation promotes metastasis in a mouse model of follicular thyroid carcinoma. *Endocrinology*. 2005;146:4456–4463.
20. **Furumoto H, Ying H, Chandramouli GV, et al.** An unliganded thyroid hormone β receptor activates the cyclin D1/cyclin-dependent kinase/retinoblastoma/E2F pathway and induces pituitary tumorigenesis. *Mol Cell Biol*. 2005;25:124–135.
21. **Cohen P, Zhao C, Cai X, et al.** Selective deletion of leptin receptor in neurons leads to obesity. *J Clin Invest*. 2001;108:1113–1121.
22. **Maffei M, Halaas J, Ravussin E, et al.** Leptin levels in human and rodent: measurement of plasma leptin and ob RNA in obese and weight-reduced subjects. *Nat Med*. 1995;1:1155–1161.
23. **Khandekar MJ, Cohen P, Spiegelman BM.** Molecular mechanisms of cancer development in obesity. *Nat Rev Cancer*. 2011;11:886–895.
24. **Scherer PE, Williams S, Fogliano M, Baldini G, Lodish HF.** A novel serum protein similar to C1q, produced exclusively in adipocytes. *J Biol Chem*. 1995;270:26746–26749.
25. **Yu H, Pardoll D, Jove R.** STATs in cancer inflammation and immunity: a leading role for STAT3. *Nat Rev Cancer*. 2009;9:798–809.
26. **Park EJ, Lee JH, Yu GY, et al.** Dietary and genetic obesity promote liver inflammation and tumorigenesis by enhancing IL-6 and TNF expression. *Cell*. 2010;140:197–208.
27. **Pearson G, Robinson F, Beers Gibson T, et al.** Mitogen-activated protein (MAP) kinase pathways: regulation and physiological functions. *Endocr Rev*. 2001;22:153–183.
28. **Alvarez JV, Febbo PG, Ramaswamy S, Loda M, Richardson A,**

Frank DA. Identification of a genetic signature of activated signal transducer and activator of transcription 3 in human tumors. *Cancer Res*. 2005;65:5054–5062.
29. **Zhang X, Yue P, Page BD, et al.** Orally bioavailable small-molecule inhibitor of transcription factor Stat3 regresses human breast and lung cancer xenografts. *Proc Natl Acad Sci USA*. 2012;109:9623–9628.
30. **Venkatesh YS, Ordonez NG, Schultz PN, Hickey RC, Goepfert H, Samaan NA.** Anaplastic carcinoma of the thyroid. A clinicopathologic study of 121 cases. *Cancer*. 1990;66:321–330.
31. **Han JM, Bae Kim W, Kim TY, et al.** Time trend in tumour size and characteristics of anaplastic thyroid carcinoma. *Clin Endocrinol (Oxf)*. 2012;77:459–464.
32. **Spires JR, Schwartz MR, Miller RH.** Anaplastic thyroid carcinoma. Association with differentiated thyroid cancer. *Arch Otolaryngol Head Neck Surg*. 1988;114:40–44.
33. **Yue P, Turkson J.** Targeting STAT3 in cancer: how successful are we? *Expert Opin Investig Drugs*. 2009;18:45–56.
34. **Paz-Filho G, Lim EL, Wong ML, Licinio J.** Associations between adipokines and obesity-related cancer. *Front Biosci*. 2011;16:1634–1650.
35. **Cheng SP, Chi CW, Tzen CY, et al.** Clinicopathologic significance of leptin and leptin receptor expressions in papillary thyroid carcinoma. *Surgery*. 2010;147:847–853.
36. **Cheng SP, Yin PH, Hsu YC, et al.** Leptin enhances migration of human papillary thyroid cancer cells through the PI3K/AKT and MEK/ERK signaling pathways. *Oncol Rep*. 2011;26:1265–1271.
37. **Huang SP, Wu MS, Shun CT, et al.** Interleukin-6 increases vascular endothelial growth factor and angiogenesis in gastric carcinoma. *J Biomed Sci*. 2004;11:517–527.
38. **Mentor-Marcel RA, Bobe G, Barrett KG, et al.** Inflammation-associated serum and colon markers as indicators of dietary attenuation of colon carcinogenesis in ob/ob mice. *Cancer Prev Res (Phila)*. 2009;2:60–69.
39. **Fenton JI, Birmingham JM.** Adipokine regulation of colon cancer: adiponectin attenuates interleukin-6-induced colon carcinoma cell proliferation via STAT-3. *Mol Carcinog*. 2010;49:700–709.